Observation-assisted optimal control of quantum dynamics

Feng Shuang, Alexander Pechen, Tak-San Ho and Herschel Rabitz

Department of Chemistry, Princeton University, Princeton, NJ 08544

(Dated: September 6, 2006)

Abstract

This paper explores the utility of instantaneous and continuous observations in the optimal control of quantum dynamics. Simulations of the processes are performed on several multilevel quantum systems with the goal of population transfer. Optimal control fields are shown to be capable of cooperating or fighting with observations to achieve a good yield, and the nature of the observations may be optimized to more effectively control the quantum dynamics. Quantum observations also can break dynamical symmetries to increase the controllability of a quantum system. The quantum Zeno and anti-Zeno effects induced by observations are the key operating principles in these processes. The results indicate that quantum observations can be effective tools in the control of quantum dynamics.

I. INTRODUCTION

The control of quantum processes is actively being pursued theoretically[1–3] and experimentally[4, 5] with a variety of control scenarios[6–10]. An increasing number of successful control experiments, including in complex systems[11–18], employ closed-loop optimal control[19]. The latter experiments commonly aim to enhance the yield of a particular desired final state, where a measurement of the quantum system is only performed after the evolution is over. Utilizing quantum observations *during* the control process may offer an opportunity to enhance performance[20, 21]. Recent studies[22, 23] also have shown that controlled quantum dynamics can operate in the presence of significant field noise and decoherence, and even cooperate with them under suitable circumstances. This paper will demonstrate that analogous control cooperation can occur between the actions of applied external fields and observations with both aiming to manipulate the system's quantum dynamics.

A characteristic feature of quantum mechanics is that the performance of a measurement unavoidably affects the subsequent system dynamics. A well known manifestation of this observation driven back action is the uncertainty principle[24]. A direct influence of a measurement is revealed through a change in the system state. In the von Neuman view of quantum mechanics, an instantaneous measurement projects the state of the system onto an eigenstate of the observable operator[25]. The measurement process induces irreversible dynamics and results in a lack of system coherence, corresponding to the off-diagonal matrix elements of the density matrix decaying to zero or the phase of the wavefunction amplitudes being randomized.

This paper is concerned with measurements carried out over a period of time. One of the earliest approaches to continuous quantum measurements was suggested by Feynman in terms of path integrals[26]. When measurements are performed the Feynman propagator is modified by restricting the paths to cross (or not to cross) certain space-time regions. An approximate technique was developed by Mensky[27] who incorporated Gaussian cut-offs in the phase space path integrals and showed its equivalence to the phenomenological master equation approach for open quantum system dynamics using models of system-environment coupling[28].

Prevention of a quantum system's time evolution by means of repetitive, frequent ob-

servations or continuous observations of the system's state is called the quantum Zeno effect (QZE). The QZE was proposed by Misra and Sudarshan[29] and was experimentally demonstrated[30] in a repeatedly measured two-level system undergoing Rabi oscillations. A time-dependent observable projection operator inducing up to 100% transfer from one state to another state[31] is called the quantum anti-Zeno effect (QAZE). The impacts of QZE and QAZE operations are the key processes explored in this paper to help control quantum dynamics.

This paper explores the scope of what might be gained in terms of better control performance from utilizing suitable observations. The practical means of executing observations in this fashion will be the subject of future works. The remainder of the paper is broken down the following way. Section II reviews the main concepts of performing instantaneous and continuous measurements, which are utilized in this paper. Section III presents the model system, and Section IV presents simulations of the closed-loop management of quantum dynamics assisted by measurements. A brief summary of the findings is given in Section V.

II. QUANTUM OBSERVATIONS

A. Instantaneous observations

An ideal instantaneous measurement occurs at one point of time, or a sequence of such observations can follow each other at different times[25]. An instantaneous measurement may be characterized by a set of projectors $\{P_i\}$ satisfying conditions of completeness and orthogonality

$$\sum_k P_k = 1, \quad P_i P_j = 0 \text{ for } i \neq j. \tag{1}$$

The instantaneous measurement converts the state ρ into the state ρ',

$$\rho' = \sum_k P_k \rho P_k. \tag{2}$$

We may also observe a physical quantity represented by the operator A,

$$A = \sum_i a_i \left|a_i\right\rangle \left\langle a_i\right|, \tag{3}$$

where a_i and $|a_i\rangle$ are the i-th eigenvalue and eigenstate, respectively, of the observable operator A, and the density matrix maybe expressed in the form

$$\rho = \sum_{k,j} \rho_{kj} |a_k\rangle \langle a_j| . \tag{4}$$

When a measurement of A is performed, the reduction

$$\rho_{kj} \to 0, \text{ for } a_k \neq a_j \tag{5}$$

occurs, thereby destroying the coherence between nondegenerate states of operator A. If A has no degenerate eigenstates, then ρ will contain only diagonal elements after an instantaneous quantum measurement

$$\rho \to \sum_{k} \rho_{kk} |a_k\rangle \langle a_k| . \tag{6}$$

If a projection operator P is observed, it's easy to deduce from Eq. (2) that after the observation process, the density matrix is transformed to ρ' given by

$$\rho' = P\rho P + (1-P)\rho(1-P) \tag{7a}$$

$$= \rho - [P,[P,\rho]] . \tag{7b}$$

The operation $[P,[P,\rho]]$ may be viewed as the "kick" resulting from the instantaneous observation of the projection operator P.

B. Continuous observations

The employment of restricted path integrals and master equations (ME) form two equivalent techniques in the theory of continuous quantum measurements[27]. For simplicity, we adopt the ME formalism. With a continuous measurement of a single observable A the ME takes the form [28]:

$$\dot{\rho} = -i[H,\rho] - \frac{1}{2}\kappa[A,[A,\rho]] . \tag{8}$$

Here, H is the Hamiltonian of the measured system, and κ indicates the "strength" of the observation. Equation (8) is similar to the equation describing a system interacting with the

environment. The first term in Eq. (8) describes the propagation of the free system, while the second term provides the decay of the off-diagonal matrix elements, such that

$$\frac{\partial}{\partial t}\left\langle a_i|\rho|a_j\right\rangle = -i\left\langle a_i\right|\left[H,\rho\right]\left|a_j\right\rangle - \frac{1}{2}\kappa\left(a_i - a_j\right)^2\left\langle a_i|\rho|a_j\right\rangle . \tag{9}$$

III. THE MODEL SYSTEM

The effect of measurements on controlled quantum dynamics is explored here in the context of population transfer in several multilevel systems characterized by the Hamiltonian,

$$H = H_0 - \mu E(t), \tag{10a}$$

$$H_0 = \sum_{\upsilon} \varepsilon_{\upsilon} \left|\upsilon\right\rangle \left\langle\upsilon\right| , \tag{10b}$$

where $|\upsilon\rangle$ is an eigenstate of H_0 and ε_{υ} is the associated field-free eigenenergy, and μ is the dipole operator. The control field $E(t)$ is taken to have the following form which may be implemented in the laboratory[32],

$$E(t) = s(t)\sum_{l}^{M} A_l \cos\left(\omega_l t + \theta_l\right), \tag{11a}$$

$$s(t) = \exp\left[-\left(t - T_f/2\right)^2/2\sigma^2\right], \tag{11b}$$

where $\{\omega_l\}$ are the M allowed resonant transition frequencies of the system and $s(t)$ is the pulse envelope function. The controls are the amplitudes $\{A_l\}$ and phases $\{\theta_l\}$.

Closed-loop control simulations will be performed to model a laboratory circumstance with the cost function:

$$J\left[E(t)\right] = \left|O\left[E(t)\right] - O_T\right|^2 + \alpha F, \tag{12a}$$

$$F = \sum_{l}\left(A_l\right)^2 , \tag{12b}$$

where O_T is the target value (expressed as a percent yield) and

$$O\left[E(t)\right] = \mathrm{Tr}[\rho(T_f)\hat{O}] \tag{13}$$

is the outcome produced by the field $E(t)$ at time T_f, and F is the fluence of the control field whose contribution is weighted by the constant, $\alpha > 0$. In the present work, $\hat{O} = \left|\Psi_f\right\rangle\left\langle\Psi_f\right|$

is a projection operator for transferring population into the target state $|\Psi_f\rangle$. The goal of this study is to explore the role that observations can play in aiding the control process and possibly reducing the fluence of $E(t)$ to more effectively achieve the desired final state.

IV. OBSERVATIONS SERVING AS CONTROLS

In this section, we numerically investigate four simple model systems in Fig. 1 to explore the use of observations in the control of quantum dynamics. In model 1, the control field is optimized and shown to be capable of fighting against the effect of instantaneous observations of different operators when they act as disturbances. The optimal control fields are also capable of cooperating with the observation of the dipole to attain a better value for the objective, even when the desired target yield is large. In model 2, the control field is fixed but the instantaneous observed operators are optimized. It is shown how the presence of even a non-optimal control field can help the observation processes meet the target yield. Quantum observations are used to break the dynamical symmetry in model 3, and the optimized continuous observations are shown to assist in making the control process more effective. In model 4, continuous observation is used to avoid population loss into an undesired state. In the first two models, the QAZE is used to induce population transfer, while the QZE is the operating process in models 3 and 4 used to prohibit population transfer. In all the illustrations a genetic algorithm[33] is employed to optimize the control fields and observations.

A. Model 1

This model uses the five-level system in Fig. 1(a) with eigenstates $|i\rangle$, $i = 0, \cdots, 4$ of the field free Hamiltonian H_0, having only nearest neighbor transitions with frequencies $\omega_{01} = 1.511$, $\omega_{12} = 1.181$, $\omega_{23} = 0.761$, and $\omega_{34} = 0.553$ in rad fs^{-1}, and associated transition dipole moments $\mu_{01} = 0.5855$, $\mu_{12} = 0.7079$, $\mu_{23} = 0.8352$ and $\mu_{34} = 0.9281$ in 1.0×10^{-30} C m. The target time is $T_f = 200$ fs, the pulse width in Eq. (11) is $\sigma = 30$ fs, and the weight coefficient in Eq. (12a) is $\alpha = 0.05$. The control objective is to transfer population from the initially prepared ground state $|0\rangle$ to the highest excited state $|4\rangle$, such that $\hat{O} = |4\rangle\langle 4|$ in Eq. (13). As a reference control case, we first determine the optimal control field without

any observations. Figure 2 depicts the amplitude and power spectrum of control field. A population transfer of 98.44% is achieved in the target state by the optimal control field which has the fluence 0.063. The fields in all of the illustrations in this paper have general structure similar to that in Fig. 2 due to the imposed form in Eq. (11), and these other fields will not be explicitly shown.

Assuming that for some auxiliary purpose we need to detect a physical quantity A at the middle of dynamical evolution at

$$T_m = \frac{T_f}{2}, \tag{14}$$

Table I shows how the optimally determined control fields (i.e., each observation has a distinct optimal field of the form in Eq. (11)) fight against the observation of the dipole μ, the energy H_0 and the population of each level

$$P_k = |k\rangle \langle k| \tag{15}$$

with $k = 0, \cdots, 4$. The second column of Table I indicates that the control field can fight very effectively with the disturbance caused by the individual quantum observations. Note that the results for population observations (the third column of Table I with P_k, $k = 0, \cdots, 4$) are all near zero, which reveals the mechanism employed by each control field to fight against its associated observation: the control field $E_k(t)$ associated with the observation operator P_k drives the system to a state $\rho(T_m) = |\psi\rangle \langle\psi|$ that is nearly orthogonal to the observed state $|k\rangle$,

$$\langle\psi|k\rangle \approx 0, \tag{16}$$

such that

$$[P_k, [P_k, \rho(T_m)]] \approx 0. \tag{17}$$

This behavior assures that the observation of P_k has little effect on the system state, or equivalently the "kick" from the observation disappears from Eq. (7b). After checking the results of observing the energy and dipole, we find a similar mechanism: their observed values at T_m are all nearly equal to an eigenvalue of the observed operators, which means that the control field drives the system to an eigenstate of the observed operators at T_m, again so that the observation has little effect on the system state. It is evident in this case that the deleterious impact of any instantaneous observation can be corrected because a suitable control field can drive model 1 to any state. The fourth column in Table I uses the

optimal fields determined in the presence of the observation, but the dynamics are carried out in the end without the observation being present. The very similar yields in the second and fourth columns are consistent with the mechanism indicated above. The last column in Table I shows that fighting against the disturbance created by the observation increases the control field fluence, whose values depend on the particular observation operator. These results collectively indicate that in the present model when seeking a high target yield the most efficient strategy for the control field is to fight the impact of the observation, which is acting as a disturbance disruptive to the control goal.

The observation of the dipole can have the dual competitive role of destroying the coherence of the system, while also inducing population transfer. A calculation shows that performance of an observation of the dipole μ without the control field being present can induce 22.19% population transfer from the initial state to the target state. Table II describes how the optimal control fields work with an observation of the dipole μ to reach different posed target yields. The second column shows that the target yield can be reached in all the cases, with some lose in achieved fidelity at the highest demanded yield of $O_T = 100\%$. In order to reveal the contributions of the observations upon the optimally controlled dynamics, the third column of Table II shows the yield from the field alone without the observation being made, yet with the field determined in the presence of the observation. Comparison of the second and third column in Table II shows that a remarkable degree of cooperation is found when the expected target yield lies in the range greater than 22.19% up to $\sim 50\%$, and the effect is even evident at the 70% target yield. For example, at the target yield of $O_T = 40\%$, the observation and optimal field alone, respectively, produce yields of 22.19% and 2.69%. But, the same field operating in the presence of the observation produces a yield of 39.82%. This behavior indicates that the field is cooperating with the observation to more effectively achieve the posed goal. Above a target yield of $\sim 80\%$, the field works to fight against the observation acting as a disturbance. The fourth column of Table II shows that the fluence generally follows this behavior. Below a target yield of $\sim 70\%$ and higher than 22.19%, the reduced fluence with the observation being present shows the enhanced control efficiency. Above that value the observation increasingly acts as a disturbance, which calls for an enhanced field fluence to fight against it.

B. Model 2

Model 2 has the same Hamiltonian and dipole elements as model 1, but we concentrate on studying the effects of a sequence of instantaneous observations treated now as controls for the population transfer. Again, the object is to transfer population from level 0 to level 4 at the target time $T_f = 200$ fs. We assume that any projection operator may be observed in a suitably performed experiment. A sequence of N instantaneous projection observations, specified by the operators

$$P_k = |\psi_k\rangle \langle\psi_k| \,,\, k = 1, \cdots, N, \tag{18a}$$

$$|\psi_k\rangle = \sum_{j=0}^{4} a_{jk} |j\rangle \,, \quad \sum_{j=0}^{4} |a_{jk}|^2 = 1 \tag{18b}$$

are performed at equally spaced time intervals,

$$t_k = \frac{k}{N+1} T_f, \, k = 1, \cdots, N, \tag{19}$$

respectively. The variables subjected to optimization are the complex coefficients $\{a_{jk}\}$ in the projection operators of Eq. (18). A control field, of the form Eq. (11), is utilized in some of the simulations, but the amplitudes and phases are picked *a priori* without any attempt at optimization. At first, the control field is turned off and the objective functional,

$$J\left[\mathbf{P}_N\right] = \left|O\left[\mathbf{P}_N\right] - 100\%\right|^2, \tag{20}$$

is optimized with respect to the coefficients $\{a_{jk}\}$ in the N observed operators

$$\mathbf{P}_N = \left(P_1, \cdots, P_N\right). \tag{21}$$

In Eq.(20) $O\left[\mathbf{P}_N\right]$ is the population yield attained from the observations without the control field. The second column of Table III shows the largest attainable population transfer with different numbers of optimized observations when the control field is off. It has been proved that the QAZE induced by suitable time-dependent measurements can fully transfer population to a target state in the frequent measurement limit[31], $\lim_{N\to\infty} O\left[\mathbf{P}_N\right] = 100\%$. We now introduce a weak control field of the form in Eq. (11) with all of the amplitudes being 0.07 and phases set at 0.0. The target time is $T_f = 200$ fs, and the pulse width in Eq. (11) is $\sigma = 30$ fs. This fixed non-optimal control field can only drive 12.93% of the

population to target state when acting alone (i.e., without observation). The objective is now a functional of both the control field and measured operators,

$$J\left[E\left(t\right),\mathbf{P}_N\right]=\left|O\left[E(t),\mathbf{P}_N\right]-100\%\right|^2, \tag{22}$$

but still only the observation operators $\mathbf{P}_N$ are optimized. The third column in Table III shows the attained population transfer induced by both the control field and the optimized observations acting together. The contribution from the observations acting alone is listed in the fourth column. A high degree of cooperation between the control field and observation is found. For example, for $N=5$ the observations carried out alone produce a yield of 20.46% and the yield from the non-optimal control field alone is 12.93%, but the yield from both acting together is 79.22%, much larger than their simple summation. Table III indicates that when $N<9$, the presence of the control field is helpful for achieving a higher yield. Further numerical simulations show that, when $N\geq 9$, the presence of the control field becomes less helpful, which reflects the strength of observations acting alone as controls. This behavior may be confirmed by an analytical assessment[34, 35] of $O\left[P_N\right]$, which proves that, when $N\geq 9$, the maximum population transfer induced by N observations is larger than 80%.

C. Model 3

Model 3 in Fig. 1(b) is a high symmetry three-level system with the Hamiltonian H_0 and dipole μ given by

$$H_0=\begin{pmatrix}1&0&0\\0&2&0\\0&0&3\end{pmatrix},\ \mu=\begin{pmatrix}0&1&0\\1&0&1\\0&1&0\end{pmatrix}. \tag{23}$$

The system is initially prepared in its ground state $|0\rangle$, and the objective is to transfer the population to state $|1\rangle$ at target time $T_f=200$ fs. If only a dipole-coupled external field is employed, the high symmetry in H_0 and μ implies that the system is not fully controllable, and by inspection at most 50% of the population maybe be transferred to state $|1\rangle$. This assessment can be made rigorous in the following analysis. It has been proved[36] that there is a hidden dynamical symmetry in this system,

$$\left|C_0\left(t\right)C_2\left(t\right)-\frac{C_1^2\left(t\right)}{2}\right|=\left|C_0\left(0\right)C_2\left(0\right)-\frac{C_1^2\left(0\right)}{2}\right|=0, \tag{24}$$

where $C_k(t)$, $k = 1, 2, 3$ are complex coefficients of the system wavefunction

$$\psi(t) = \sum_{k=0}^{2} C_k(t) |k\rangle . \tag{25}$$

Rewriting Eq. (24) in terms of density matrix elements gives

$$\rho_{00}(t) \rho_{22}(t) = \frac{\rho_{11}^2(t)}{4}. \tag{26}$$

The following inequality based on Eq. (26) shows that no more than 50% of the population can be driven from its ground state $|0\rangle$ to the state $|1\rangle$

$$\rho_{11}(t) = 2\sqrt{\rho_{00}(t) \rho_{22}(t)} \leq \rho_{00}(t) + \rho_{22}(t) = 1 - \rho_{11}(t) . \tag{27}$$

To explore if observations can break the 50% yield limit, first a simple instantaneous observation and then a time-dependent continuous observation is applied. The control field is a simple resonant pulse,

$$\begin{cases} E(t) = A \cos t, \; 0 \leq t \leq T_f, \\ E(t) = 0, \qquad \text{otherwise}, \end{cases} \tag{28}$$

where only the amplitude A is adjusted for optimization.

First, an instantaneous observation is performed at the middle of the control $T_m = T_f/2$. Table IV shows various control yields when different instantaneous observations are carried out, where P_k is the population measurement operator in Eq. (15). The simulation shows that an instantaneous population observation of state $|0\rangle$ or $|2\rangle$ can increase the population transfer to the target state $|1\rangle$, but at the expense of requiring stronger control fields. In contrast, an observation of the target state population is not helpful. This behavior can be explained by the broken dynamical symmetry induced by the observation of state $|0\rangle$ or $|2\rangle$, but this outcome will not be the case from observation of state $|1\rangle$. An analytical treatment[35] shows that the maximum attainable population transfer to the level $|1\rangle$ by a coherent field assisted from measuring P_0 or P_2 is $\sqrt{2}/2 = 70.7\%$, which is closely approximated by the value of $\simeq 67\%$ in Table IV.

Now consider carrying out time-dependent continuous observations together with a control field $E(t)$ having the form in Eq. (28), where the density matrix satisfies

$$\dot{\rho} = -i [H_0 - \mu E(t), \rho] - \frac{1}{2} \kappa(t) [P, [P, \rho]] . \tag{29}$$

Here the observation strength $\kappa(t)$ is allowed to be time-dependent, and a simple form of $\kappa(t)$ is adopted as it proved to be sufficient in the control of model 3:

$$\kappa(t) = \begin{cases} \gamma, & T_1 < t < T_2, \\ 0, & \text{otherwise.} \end{cases} \tag{30}$$

In this case the objective functional J is optimized with respect to not only the control field parameter A in Eq. (28), but also the observation strength γ and time interval T_1, T_2,

$$J[A, \gamma, T_1, T_2] = |O[A, \gamma, T_1, T_2] - 100\%|^2 + \alpha A^2. \tag{31}$$

The coefficient α in Eq. (31) is 0.01. In the simulation, the observation strength γ was optimized over the range from 0.0 to 5.0. Table V shows that with the help of the optimized continuous observations of the population in state $|0\rangle$ or $|2\rangle$, the control field can induce almost 100% population transfer between the initial state $|0\rangle$ and target state $|1\rangle$. As expected, observation of the state $|1\rangle$ is not helpful. Figure 3(a) shows the state populations when the optimized continuous observation is on state $|0\rangle$ and Fig. 3(b) shows the state populations when the optimized continuous observation is on state $|2\rangle$. The results in Fig. 3 indicate that the observation of P_0 or P_2 eliminate population from the state being observed, and the three-level system becomes an effective two-level system in the time interval $T_1 < t < T_2$. This behavior is consistent with the observation acting under the QZE. In both cases γ adopts its maximum value of 5.0 under optimization to evidently take full advantage of the QZE. The simulations with this simple model show that observations can fundamentally alter the effective dynamical structure of a quantum system. Naturally, for more complex systems, additional specially tailored time-dependent observations may be required for optimal impact on the controlled dynamics.

D. Model 4

The structure of model 4 is given in Fig. 1(c), and the objective is to transfer population from level 0 to level 3. There are two degenerate transitions, $\omega_{11'} = \omega_{23} = 0.8$, and the other transition frequencies are $\omega_{01} = 3.3$, $\omega_{12} = 2.6$. The non-zero dipole elements are: $\mu_{01} = 0.13$, $\mu_{12} = 0.15$, $\mu_{23} = 0.23$ and $\mu_{11'} = 0.21$. The control field has the form of Eq. (11) with the resonant three amplitudes and phases subjected to optimization. The target time is $T_f = 200$ fs, the pulse width in Eq. (11) is $\sigma = 30$ fs and the weight coefficient in

Eq. (12a) is $\alpha = 0.01$. The simulation in the first row of Table VI shows that under these conditions, with no observation, the control field can only drive 71.96% of population to the target state, mainly because some population is locked in the undesired state $|1'\rangle$. If a constant continuous observation of the population of state $|1'\rangle$ is carried out, the dynamics of model 4 is described by following equation:

$$\dot{\rho} = -i\left[H_0 - \mu E\left(t\right), \rho\right] - \frac{1}{2}\kappa\left[P_{1'}, \left[P_{1'}, \rho\right]\right], \tag{32a}$$

$$P_{1'} = \left|1'\right\rangle\left\langle 1'\right|. \tag{32b}$$

Table VI shows that increasing κ results in a reduction of the population in state $|1'\rangle$. The phenomena can be explained by the QZE: the strong continuous measurement of state $|1'\rangle$ prohibits population transfer between state $|1\rangle$ and $|1'\rangle$ and avoids population loss to the undesired state $|1'\rangle$, thereby increasing the population in the target state. In all the cases in Table VI the fluence of the control field remains approximately the same at F $\simeq$ 0.57, despite the fact that some of the amplitudes A_l in Eq. (11a) changed to some degree as κ varied. Population loss to undesired states is commonly encountered in the practical control of quantum dynamics. This model shows a mechanism to avoid the loss.

V. CONCLUSIONS

This paper discusses observations serving as indirect controls in the manipulation of quantum dynamics. In this context, the field entering the Hamiltonian can be viewed as a direct control. Instantaneous and continuous observations were both considered along with control fields to manipulate population transfer. The simulations show that suitable observations can be very helpful in the manipulation of quantum dynamics. In favorable cases the optimal control field can cooperate with observations to achieve the target more effectively, even when the objective yield is large. In turn, optimal observations can work with an existing or constrained control field to transfer more population from an initial state to a target state. Observations can break dynamical symmetry to increase controllability as well as prohibit transfer of amplitude to undesired states. The QZE and QAZE are the key operational processes associated with the observations to assist the control field to more effectively achieve the target objective. The performance of optimal observations hopefully

will become routine with advancing technology, as observations can be powerful tools in the control of quantum dynamics.

Acknowledgments

The authors acknowledge support from the NSF, DARPA and ARO-MURI.

---

[1] S. A. Rice and M. Zhao, *Optical Control of Molecular Dynamics* (Wiley, New York, 2000).

[2] H. Rabitz, Theor. Chem. Acc. **109**, 64 (2003).

[3] M. Shapiro and P. Brumer, *Principles of the Quantum Control of Molecular Processes* (John Wiley, New York, 2003).

[4] I. Walmsley and H. Rabitz, Phys. Today **56**, 43 (2003).

[5] T. Brixner, N. H. Damrauer, and G. Gerber, in *Advances in Atomic, Molecular, and Optical Physics*, edited by B. Bederson and H. Walther (Academic, San Diego, CA, 2001), vol. 46, pp. 1–54.

[6] A. P. Peirce, M. A. Dahleh, and H. Rabitz, Phys. Rev. A **37** (1988).

[7] R. Kosloff, S. A. Rice, P. Gaspard, S. Tersigni, and D. J. Tannor, Chem. Phys. **139** (1989).

[8] M. Shapiro and P. Brumer, J. Chem. Phys **84** (1986).

[9] U. Gaubatz, P. Rudecki, S. Schiemann, and K. Bergmann, J. Chem. Phys. **92**, 5363 (1990).

[10] M. N. Kobrak and S. A. Rice, Phys. Rev. A **57** (1998).

[11] A. Assion, T. Baumert, M. Bergt, T. Brixner, B. Kiefer, V. Seyfried, M. Strehle, and G. Gerber, Science **282**, 919 (1998).

[12] M. Bergt, T. Brixner, B. Kiefer, M. Strehle, and G. Gerber, J. Phys. Chem. A **103**, 10381 (1999).

[13] J. Kunde, B. Baumann, S. Arlt, F. Morier-Genoud, U. Siegner, and U. Keller, Appl. Phys. Lett. **77**, 924 (2000).

[14] R. Bartels, S. Backus, E. Zeek, L. Misoguti, G. Vdovin, I. P. Christov, M. M. Murnane, and H. C. Kapteyn, Nature **406**, 164 (2000).

[15] T. Brixner, N. H. Damrauer, P. Niklaus, and G. Gerber, Nature (London) **414**, 57 (2001).

[16] R. J. Levis, G. M. Menkir, and H. Rabitz, Science **292**, 709 (2001).

[17] J. Herek, W. Wohlleben, R. Cogdell, D. Zeidler, and M. Motzkus, Nature **417**, 533 (2002).

[18] C. Daniel, J. Full, L. González, C. Lupulescu, J. Manz, A. Merli, Š. Vajda, and L. Wöste, Science **299**, 536 (2003).

[19] R. S. Judson and H. Rabitz, Phys. Rev. Lett. **68**, 1500 (1992).

[20] J. Gong and S. A. Rice, J. Chem. Phys. **120**, 9984 (2004).

[21] M. Sugawara, J. Chem. Phys. **123**, 204115 (2005).

[22] F. Shuang and H. Rabitz, J. Chem. Phys. **121**, 9270 (2004).

[23] F. Shuang and H. Rabitz, J. Chem. Phys. **124**, 154105 (2006).

[24] M. B. Mensky, *Continuous Quantum Measurements and Path Integrals* (IOP Publishing, Bristol and Philadelphia, 1993).

[25] V. Neumann, *Mathematical foundations of quantum mechanics* (Princeton University Press, Princeton, 1955).

[26] R. P. Feynman, Rev. Mod. Phys. **20**, 367 (1948).

[27] M. Mensky, Phys. Lett. A **196**, 159 (1994).

[28] D. F. Walls and G. J. Milburn, *Quantum Optics* (Springer, Berlin, 1994).

[29] B. Misra and E. Sudarshan, J. Math. Phys. **18**, 756 (1977).

[30] W. M. Itano, D. J. Heinzen, J. J. Bollinger, and D. J. Wineland, Phys. Rev. A **41**, 2295 (1990).

[31] A. P. Balachandran and S. M. Roy, Phys. Rev. Lett. **84** (2000).

[32] A. Lindinger, S. M. Weber, C. Lupulescu, F. Vetter, M. Plewicki, A. Merli, L. Woste, A. F. Bartelt, and H. Rabitz, Phys. Rev. A **71**, 013419 (2005).

[33] D. E. Goldberg, *Genetic Algorithms in Search, Optimization, and Machine Learning* (Addison-Wesley, Reading, MA, 1989).

[34] A. Pechen, N. Il'in, F. Shuang, and H. Rabitz, submited to Phys. Rev. A, e-print quant-ph/0606187.

[35] F. Shuang, M. Zhou, A. Pechen, and H. Rabitz, in progress.

[36] G. Turinici and H. Rabitz, Chem. Phys. **267**, 1 (2001).

TABLE I. Optimal control fields fighting against the disturbance of various observations for model 1 with the goal of a high target yield $O_T = 100\%$.

A [a]	$O\left[E\left(t\right), A\right]$ [b](%)	$\mathrm{Tr}[\rho\left(T_m\right) A]$ [c]	$O\left[E\left(t\right), 0\right]$ [d](%)	F [e]
–	98.44	–	98.44	0.063
μ	92.42	0.66	94.03	0.37
H_0	85.45	3.94	85.17	1.29
P_0	97.14	*0.0037*	95.77	0.49
P_1	96.19	*0.021*	93.71	0.56
P_2	93.26	*0.055*	92.98	0.77
P_3	97.64	*0.0010*	97.27	0.78
P_4	96.59	*0.0032*	95.68	0.72

[a] The operator observed at time $T_m = T_f/2$. Here μ is the dipole; H_0 is the field-free Hamiltonian; P_k is a population projection operator for state $|k\rangle$, $k = 0, \cdots, 4$.

[b] Yield from the optimal control field and an instantaneous observation at time $T_m = T_f/2$.

[c] Observed value of operator A.

[d] Yield arising from the control field without actually performing the observation, but the control field is determined in the presence of the observation of operator A.

[e] Fluence of the control field.

TABLE II. Optimal control fields interacting with an observation of the dipole μ for model 1 with different objective yields.

O_T [a](%)	$O\left[E\left(t\right),\mu\right]$[b](%)	$O\left[E\left(t\right),0\right]$[c](%)	F^d	F_0 [e]
10	10.00	2.03×10^{-7}	0.0020	0.017
20	20.03	2.74×10^{-9}	0.00026	0.023
30	29.86	0.0052	0.0034	0.027
40	39.82	2.69	0.017	0.031
50	49.73	13.87	0.027	0.034
60	59.73	40.20	0.036	0.038
70	69.74	48.12	0.041	0.042
80	79.18	81.80	0.31	0.046
90	88.86	89.36	0.34	0.052
100	92.42	94.03	0.37	0.063

[a] Objective yield in Eq. (12a).

[b] Yield from an optimal control field and an observation of the dipole μ at time $T_m = T_f/2$.

[c] Yield arising from the control field without an observation of the dipole, but with the control field determined in the presence of an observation of the dipole.

[d] Fluence of the control field optimized with the observation present.

[e] Fluence of the control field optimized without the observation present.

TABLE III. Optimal control of model 2 with a sequence of instantaneous observations

N [a]	$O\left[\mathbf{P}\right]^{b}(\%)$	$O\left[E\left(t\right),\mathbf{P}\right]^{c}(\%)$	$O\left[0,\mathbf{P}\right]^{d}(\%)$
0	0	12.93[e]	0.00
1	50.00	56.46	11.82
3	62.50	72.60	16.90
5	71.04	79.22	20.46
7	73.72	80.61	18.22
9	80.11	80.45	19.65

[a] Number of observations N performed at times $T_k = \frac{k}{N+1}T_f$, $k = 1, \cdots N$.

[b] Yield from the optimal observations without a control field.

[c] Yield from the optimal observations in the presence of a non-optimal control field.

[d] Yield from the optimal observations without a control field, but with the optimal observations determined in the presence of non-optimal control field.

[e] The fluence of the non-optimal control field is $F = 0.0196$.

TABLE IV. Optimal control of model 3 with various instantaneous observations at time $T_m = T_f/2$.

P [a]	$O\left[E\left(t\right), P\right]$ [b](%)	$\mathrm{Tr}[\rho\left(T_m\right) P]$ [c]	$O\left[E\left(t\right), 0\right]$ [d](%)	F [e]
–	49.99	–	49.99	0.0031
P_0	66.90	0.068	46.04	0.76
P_1	49.99	0.50	50.00	0.96
P_2	66.66	0.066	46.37	0.49

[a] The operator observed at time $T_m = T_f/2$. Here P_k is a population projection operator for state $|k\rangle$, $k = 0, 1, 2$.

[b,c,d,e] Refer to Table 1.

TABLE V. Control of model 3 with an optimized continuous observation.

P [a]	$O[A, \gamma, T_1, T_2]$ [b](%)	F [e]	γ	T_1	T_2
–	49.99	0.0031	–	–	–
P_0	98.92	0.021	5.00	119.13	199.96
P_1	49.99	0.0086	0.0025	6.24	6.33
P_2	99.55	0.0037	5.00	2.55	199.24

[a] The population operator P_k is observed between time T_1 and T_2 with the strength γ. Here P_k indicates observation of the population in state $|k\rangle$, $k = 0, 1, 2$.

[b,e] Refer to Table 1.

TABLE VI. Optimal control of Model 4 with different continuous quantum observations

κ [a]	$O\left[E(t), P_{1'}\right](\%)$ [b]	$P_{1'}$ [c]
0.00	71.96	14.22
0.01	75.53	13.52
0.03	80.77	12.03
0.05	84.32	10.50
0.09	88.61	8.27
0.15	91.81	6.43
0.20	93.28	5.33
0.30	94.78	4.25

[a] Observation strength of state $|1'\rangle$; refer to Eq. (32a).

[b] Population yield in the target state $|3\rangle$ from the optimal control field and continuous observations of the population in state $|1'\rangle$.

[c] Population in the undesired state $|1'\rangle$.

Fig1. Three multilevel systems used to investigate the impact of observations in the optimally controlled quantum dynamics simulations in Sec. IV. (a) The five-level ladder configuration used for models 1 and 2. (b) Model 3 with degenerate transition frequencies $\omega_{01} = \omega_{02}$. (c) Model 4, where the two transition frequencies $\omega_{11'} = \omega_{23}$ are degenerate.

Fig2. The optimal control field and its power spectrum for model 1 without an observation being present. The field is found using the cost function in Eq. (12a) with a high expected yield of $O_T = 100\%$. The spectral features are at the system transition frequencies.

Fig3. The population evolution of model 3 driven by an optimal control field with the help of optimized continuous observations performed between time T_1 and T_2. P_k denotes the population in level k, $k = 1, 2, 3$. The observation is on state $|0\rangle$ in plot (a) and on state $|2\rangle$ in plot (b).

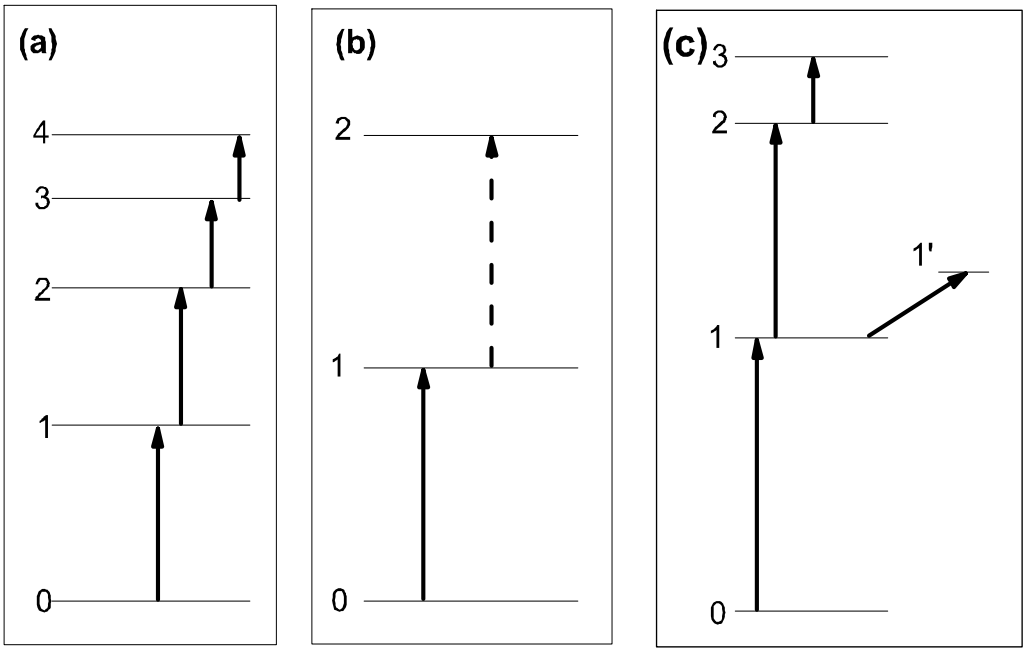

FIG. 1: F Shuang et al

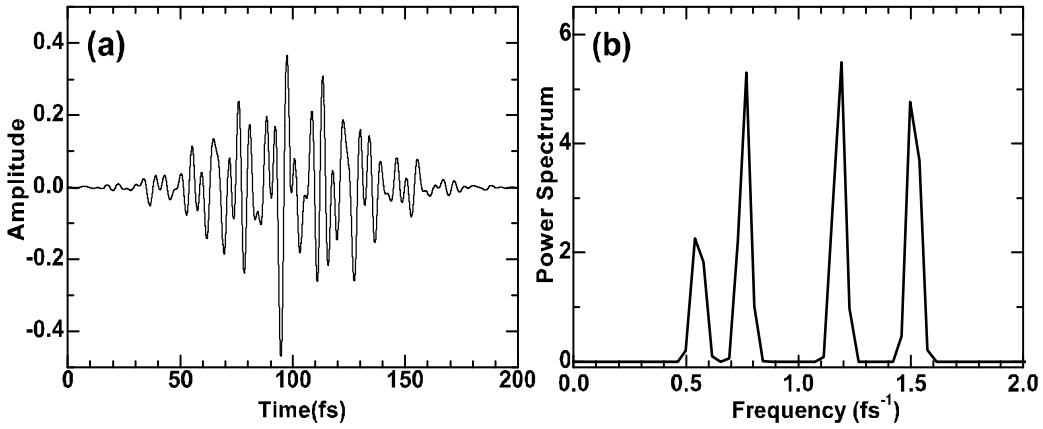

FIG. 2: F Shuang et al

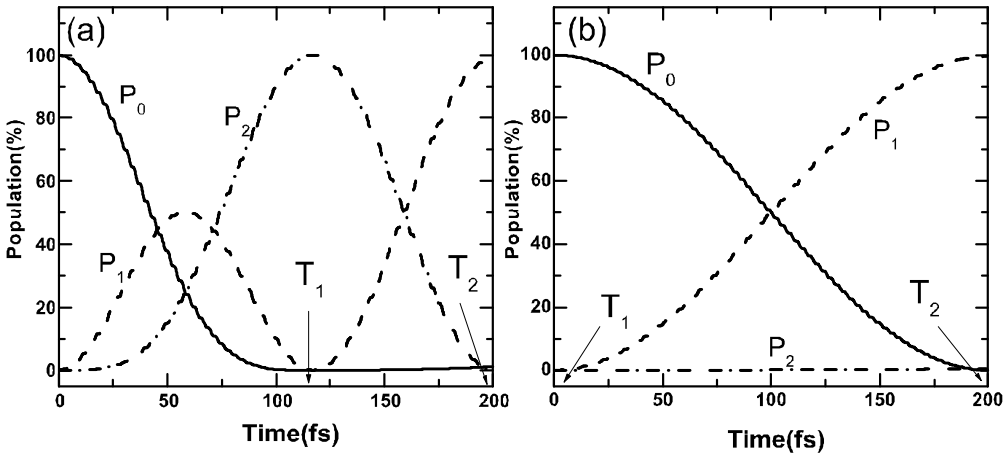

FIG. 3: F Shuang et al